

# Theoretical Analysis of Cell Separation Based on Cell Surface Marker Density

Jeffrey J. Chalmers,<sup>1</sup> Maciej Zborowski,<sup>2,3</sup> Lee Moore,<sup>3</sup> Sushim Mandal,<sup>2</sup> BingBing Fang,<sup>2</sup> Liping Sun<sup>1</sup>

<sup>1</sup>Department of Chemical Engineering, The Ohio State University, 140 West 19th Avenue, Columbus, Ohio 43210-1180; telephone: (614)-292-2727; fax: (614)-292-3769; e-mail: Chalmers.1@osu.edu

<sup>2</sup>Department of Biomedical Engineering, Case Western Reserve University, Cleveland, Ohio

<sup>3</sup>Department of Biomedical Engineering, The Cleveland Clinic Foundation, Cleveland, Ohio

Received 12 April 1997; accepted 31 October 1997

**Abstract:** A theoretical analysis was performed to determine the number of fractions a multidisperse, immunomagnetically labeled cell population can be separated into based on the surface marker (antigen) density. A number of assumptions were made in this analysis: that there is a proportionality between the number of surface markers on the cell surface and the number of immunomagnetic labels bound; that this surface marker density is independent of the cell diameter; and that there is only the presence of magnetic and drag forces acting on the cell. Due to the normal distribution of cell diameters, a "randomizing" effect enters into the analysis, and an analogy between the "theoretical plate" analysis of distillation, adsorption, and chromatography can be made. Using the experimentally determined, normal distribution of cell diameters for human lymphocytes and a breast cancer cell line, and fluorescent activated cell screening data of specific surface marker distributions, examples of theoretical plate calculations were made and discussed. © 1998 John Wiley & Sons, Inc. *Biotechnol Bioeng* 59: 10–20, 1998.

**Keywords:** surface marker density; receptor density; immunomagnetic cell separation

## INTRODUCTION

The ability to differentiate a heterogeneous cell population based solely on the expression of a surface-expressed marker has become a significant analytical technology in basic biological studies, in applied biological studies, in clinical diagnosis of disease, and in rapidly developing cell-based therapies in the treatment of human disease. Much of this development is the result of the use of antibody–fluorescent label conjugates for specific cell surface markers and the ability of fluorescent activated cell sorting (FACS) systems to separate these labeled cells. More recently, magnetic separation, based on the use of paramagnetic beads conjugated to these specific antibodies, has become quite common.

Figure 1 presents a typical cell fluorescence histogram

Correspondence to: J. J. Chalmers

Contract grant sponsors: National Institutes of Health; National Science Foundation; The Whitaker Foundation

Contract grant numbers: CA62349; BCS9258004

(cell count vs. log of fluorescence intensity, FI), from flow-cytometric analysis, of human cytotoxic T lymphocytes, labeled with a CD8 antibody–fluorescein conjugate (Zborowski et al., 1997b). As can be observed, the positive cell population (the cell counts under the "M1" line) is not a single peak, but has a large range (on the order of two orders of magnitude) of fluorescence intensities (note that the *x*-axis is logarithmic). If it is assumed that a constant proportionality exists between the cell surface marker and the fluorescence label used, and that all the cells have the same diameter, then more than two orders of magnitude in the cell surface marker density exist. However, as will be mathematically demonstrated in what follows, some of this distribution can also result from distributions in cell diameter. Shapiro (1995) noted that there are several examples of large (several orders of magnitude) nongaussian distributions of surface antigens including the distribution of CD4, CD8, and CD3 antigen density on the surface of neonatal thymus cells.

Although it is generally recognized that it would be highly desirable to be able to quantitatively correlate FI to surface marker density in FACS, numerous difficulties in obtaining uniform calibration of FI have limited routine applications (Poncelet and Carayon, 1985; Vogt et al., 1989). A number of calibration techniques have been used to quantify FI. These techniques include the use of fluorescein-labeled microbeads and fluoresceinated calf thymocyte nuclei (Fluorotrol) (Vogt et al., 1989, 1991). However, problems with uniform calibrations still impede progress in the clinical application of quantitative FI measurements (Bohmer et al., 1985; Chatelier and Ashcroft, 1987; Parks et al., 1988; Vogt et al. 1991). These problems were well quantified by Vogt et al. (1991) in a study in which calibration microbeads, Fluorotrol, and human lymphocytes stained with fluoresceinated CD4 antibodies were sent to 34 laboratories to be tested on 43 different flow cytometers. All standard curves produced strongly linear results, and the pooled results from all standards produced a best-fit curve that was close to assigned values. However, results measur-

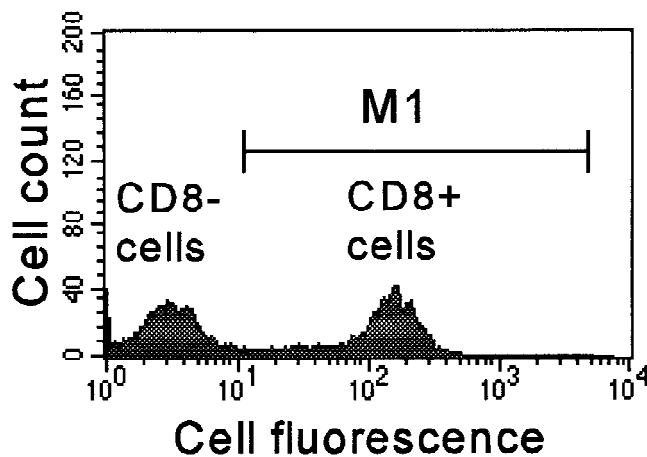


**Figure 1.** Flow-cytometric analysis of human lymphocytes labeled with a CD8 antibody-fluorescein conjugate (CD refers to “cluster of differentiation”). The CD8 antibody binds specifically to cytotoxic T cells and increases their fluorescence by about one to two orders of magnitude (CD8<sup>+</sup> cells). The rest of the cells (CD8<sup>-</sup> cells) are faintly fluorescent due to autofluorescence. M1 represents the range of CD8<sup>+</sup> cells, and the left-hand side of M1 represents the “gate” or threshold level set for binary separation. This distribution shown here represents lymphocytes enriched in CD8<sup>+</sup> cells by magnetic flow sorting (Zborowski et al., 1997b).

ing cellular FI were highly variable, with CVs ranging from 20% to 39% when calculated based on the pooled standard curve, or 3% to 9.9% when calculated based on the specific instrument standard curve. Despite considering a number of possible causes for this variability, Vogt et al. (1991) stated that “the overall variability in FI results thus remains unexplained by any single major influence addressed in our review of the data and is most likely attributable to varying combinations of smaller influences.” They further stated that laser power and optical filtration most probably contribute to this variability.

An alternative approach was taken by Poncelet and Carayon (1985) in a technique called quantitative indirect immunofluorescence assay (QIFI), which allows absolute numbers of antibody binding sites on lymphoid cells to be determined. However, this assay required the use of cell lines and radiolabeled antibodies to establish a standard curve. More recently, Poncelet et al. (1991a) reported on a modification of the original QIFI assay through the use of commercially available beads (with mouse IgG attached at varying, known densities), which can be used as secondary standards for quantitative indirect immunofluorescence assay. Using this modified technique, Poncelet et al. (1991b) determined values for the number of CD4 and CD45 antigens on normal and HIV-infected human lymphocytes. More recently, Bikoue et al. (1996), using the QIFI technique, demonstrated the linearity of the mean FI with the mouse IgG concentration on the beads. With this calibration, a more complete study of a variety of different antigen densities on human lymphoid, monocytic, and polymorphonuclear blood cells was reported. However, it should be noted that significant calibration tests were needed to obtain this result.

## Magnetic Labels

The ability to separate a cell based on magnetic forces is dependent on the ability of imparting on the cell a paramagnetic dipole moment. This is due to the fact that there is only a limited number of cells that demonstrate sufficient *intrinsic* paramagnetic moment significantly higher than that of the surrounding medium (namely water) to be of practical use in cell separation without the use of antibodies conjugated to paramagnetic markers (or other paramagnetic labeling procedures). The best known examples are erythrocytes (deoxygenated or oxidized, with trivalent iron atoms) and magnetotactic bacteria (Bazylinski et al., 1988; Meldrum et al., 1993; Okazaki et al., 1986; Pauling and Coryell, 1936). All other cells of interest have to be tagged by a magnetic label to achieve the required contrast in magnetic susceptibility between the cell and the medium. Using a commercially available antibody-paramagnetic label conjugate, and the appropriate magnetic field, a five-order-of-magnitude difference in magnetic susceptibility between a labeled and unlabeled cell can theoretically be obtained.

## Types of Paramagnetic Labels

To assist in the understanding of the paramagnetic labeling process, Figure 2 presents a schematic diagram of a typical immunomagnetic labeling complex. For the purpose of this study, the available paramagnetic labels will be classified based on their size: *particulate* (on the order of a cell diameter, typically 1 to 5  $\mu\text{m}$ ); *colloidal* (on the order of 100 nm); and *molecular* (on the order of 10 nm). Two of these types of magnetic labels, particulate and colloidal, are available commercially (Dynal AG, Oslo, Norway; Miltenyi Biotec GmbH, Bergisch Gladbach, Germany), whereas the third, molecular, is available from research labs (Zborowski et al., 1996). Two important points, which will be elaborated further, need to be made with respect to these different types of labels: (1) the physical size of the magnetic label determines the separation resolution; and (2) the magnetic moment of a magnetic label is greatly affected by the size of the bead with the large beads having orders-of-magnitude higher magnetic moment than the colloidal or molecular labels.

The large difference in the magnetic susceptibility between the unlabeled cells and the cell-bead complex (up to approximately five orders of magnitude for particulate labels) leads, in principle, to high resolution using particulate labels, such as Dynalbead M450. In practice, the resolution is decreased by a number of unwanted effects, including nonspecific binding of beads to nontarget cells, detachment of beads from target cells (sometimes with fragments of the cell membrane) due to high shear stresses created by rapidly accelerating magnetic beads, or random entrapment of cells in bead clusters (Rubbi et al., 1993). Due to these, and possibly other compounding effects, paradoxical results have been reported, showing decreasing target cell purity in the enriched fraction with increasing cell surface marker

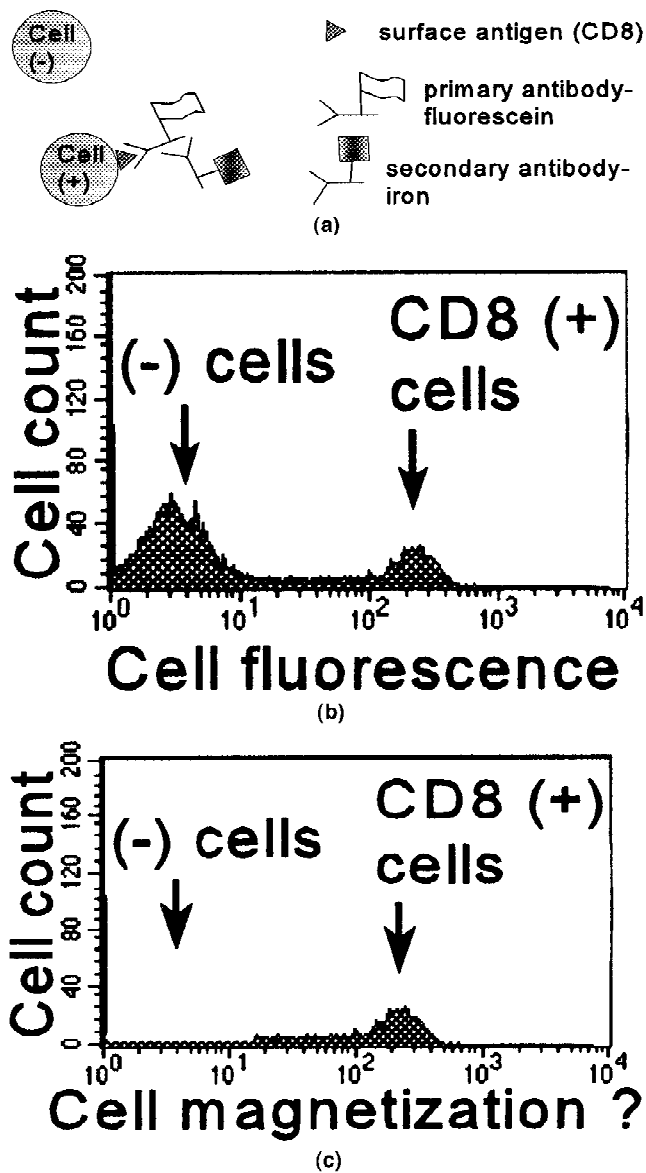


**Figure 2.** (a) Schematic rendering of immunofluorescence and immunomagnetic labeling complex. (b) Example of cell fluorescence histogram, by FACS analysis—note the presence of a negative cell population (lacking the antigenic determinant) due to cell autofluorescence. (c) Hypothetical cell magnetization histogram of the same cell sample as in (b), showing positive cell fraction and lack of negative fraction due to negligibly small intrinsic cell magnetization. The distribution of cell magnetization corresponds to the distribution of cell surface marker density, required for the *analog* separation.

density, or reappearance of the target cell phenotype in the purged cell fraction due to stripping and the resynthesis of the cell surface marker in cell culture (Mansour et al., 1992; Rubbi et al., 1993). In summary, the relatively large size of the magnetic bead limits its use to only a gross separation of cell surface marker expressors from nonexpressors (*binary* separation), without the ability to differentiate between the degree of cell surface marker expression. All of the magnetic cell separations using particulate labels are binary in nature; that is, either the cell is magnetic or it is not.

## Colloidal Magnetic Labels

Unlike the particulate labels, colloidal magnetic labels require high magnetic fields and gradients. An example of such a colloidal label is the MACS microbead, a dextran microbead doped with magnetite with a nominal diameter of 50 nm (Miltenyi Biotec) (Miltenyi et al., 1990). The small size of the MACS microbeads requires high magnetic fields and gradients to achieve sufficiently high magnetic moments and to affect cell flow in a fluid. The relatively small magnetic force,  $F_m$ , requires a short cell travel distance in solution to the deposition substrate for cell separation to occur in a realistic time interval. Such fields are provided by high-gradient magnetic separators filled with high magnetic permeability matrices (Radbruch et al., 1994). The overall performance of the MACS system is comparable to that of the Dynabead-based separation systems, with the Dynabead-based system being more efficient for negative separation, and the MACS system being more efficient for positive isolation (Manyonda et al., 1992). High purity and cell recovery of the positive cell selection becomes important to isolate rare cells for analytical purposes, such as the identification of fetal cells in the maternal blood and isolation of progenitor and stem cells from bone marrow (Busch et al., 1994; Schmitz et al., 1994).

A significant advancement in cell separation would exist if cells could be separated based on the density of the surface makers (Thomas et al., 1992). Such a separation could be defined as “analog” fractionation as opposed to the “binary” separations discussed earlier. Another way of referring to such a separation would be to “fractionate” the positive cell population into subpopulations based on cell surface marker density. A requirement of such a separation would be that there exists a proportionality between the surface marker and the paramagnetic label, just as is commonly assumed with fluorescent labels. Also, because of the problems outlined previously with particulate labels, the best type of paramagnetic label to use would be either molecular or colloidal.

As will be shown in what follows, such an “analog” fractionation will be a function of not only the cell marker density and the magnitude of the magnetic force per cell surface marker, but also the distribution of cell diameters. Consequently, experimentally determined cell diameter distributions will be presented for two types of cells, human lymphocytes (the same as presented in Fig. 1) and a human breast cancer cell line (MCF-7). In addition, FACS analysis will be presented, demonstrating the range of intensities in specific cell fluorescence for the MCF-7 cell line.

## MATERIALS AND METHODS

### Cell Types

Human peripheral blood was obtained by venipuncture from apparently healthy volunteer donors in accordance with The Cleveland Clinic Foundation Institutional Review Board

guidelines. The mononuclear fraction of human peripheral blood was obtained by centrifugation on a Ficoll cushion (Pharmacia, Uppsala, Sweden).

The human breast cancer cell line, MCF-7, was obtained from the American Type Culture Collection (ATCC, Rockville, MD) and maintained in RPMI-1640 medium (Gibco, Detroit, MI) supplemented with 10% fetal calf serum (Life Technologies, Grand Island, NY), 0.1% (v/v) insulin, 100  $\mu\text{g}/\text{mL}$  penicillin, and 100  $\mu\text{g}/\text{mL}$  streptomycin. The cells were cultured at 37°C in a humidified incubator at 6.5%  $\text{CO}_2$  and the medium was changed every 3 days.

### Cell Size Distribution

Two types of Coulter Counters (Coulter, Miami, FL) were used for cell size determination: a Model Z1 and a Multisizer IIe. To obtain a histogram using the Model Z1, after each experiment the operator manually selected the window size of interest. This window size was chosen to be 0.5  $\mu\text{m}$ , and 48 increments were used ranging from 5.125 to 19.25  $\mu\text{m}$ .

Cell size distribution for the MCF-7 cells was also determined using the Multisizer IIe apparatus. With this device sampling windows were not necessary, and the software included performed desired data analysis. With both counters, a 100- $\mu\text{m}$  aperture was used in the sampling electrode. The use of two different Coulter Counters was the result of the purchase of the Multisizer IIe after the analysis of the human lymphocytes.

### Immunofluorescence Staining of Human Lymphocytes

The cytotoxic T-lymphocyte subpopulation, characterized by the presence of the CD8 surface marker, was stained with mouse anti-human CD8 monoclonal antibody-fluorescein isothiocyanate (FITC) (B-D Immunocytometry Systems, San Jose, CA). Additional cell aliquots were stained with monoclonal antibody isotype to control for the primary antibody specificity.

### Immunofluorescence Staining of MCF-7 Cells

An indirect immunofluorescence staining procedure was used. The primary antibody used was a mouse, anti-human monoclonal antibody (MAb) to epithelial membrane antigen (EMA; Biomedica, Foster City, CA). This primary antibody was incubated with  $1.5 \times 10^6$  cells for 1 h at room temperature in 1 mL of antibody solution at either 20, 80, 140, or 200  $\mu\text{L}/\text{mL}$ . After twice being washed in  $\text{Ca}^{2+}/\text{Mg}^{2+}$ -free PBS, the cells were stained with the secondary antibody at a concentration of 1  $\mu\text{L}/\text{mL}$  for 15 min at 7°C. The secondary antibody used was a polyclonal (PAb) biotin conjugate (Coulter Immunological Co., Hialeah, FL). After secondary antibody staining, the cells were incubated in 1 mL of avidin-FITC solution (20  $\mu\text{L}/\text{mL}$ ) (Vector, Burlingame, CA) for 5 min at 7°C. The fluorescence-labeled cells were

fixed in 1 mL of 1% (v/v) paraformaldehyde, centrifuged, and resuspended in 500  $\mu\text{L}$  of PBS with 4.4% BSA.

### FACS Analysis

Flow cytometry was performed using the FACScan Analyzer and Cell Quest software (Becton-Dickinson, San Jose, CA).

### RESULTS

Figure 3a presents a graph of cell count and frequency versus cell size. As can be observed, two complete peaks and a part of a third peak are present. The peak at small diameters is most probably residual red blood cells and platelets and the large peak at approximately 7.0  $\mu\text{m}$  is lymphocytes, whereas the larger cells are most probably large lymphocytes and monocytes. This observation is in agreement with the published literature data and manufacturer's information regarding Ficoll-Paque performance. Klaus (1987) reported that the volume of lymphocytes is in the range of 120 to 290  $\mu\text{m}^3$ . Assuming lymphocytes to be perfect spheres, this returns a diameter range of approximately 6.1 to 8.2  $\mu\text{m}$ .

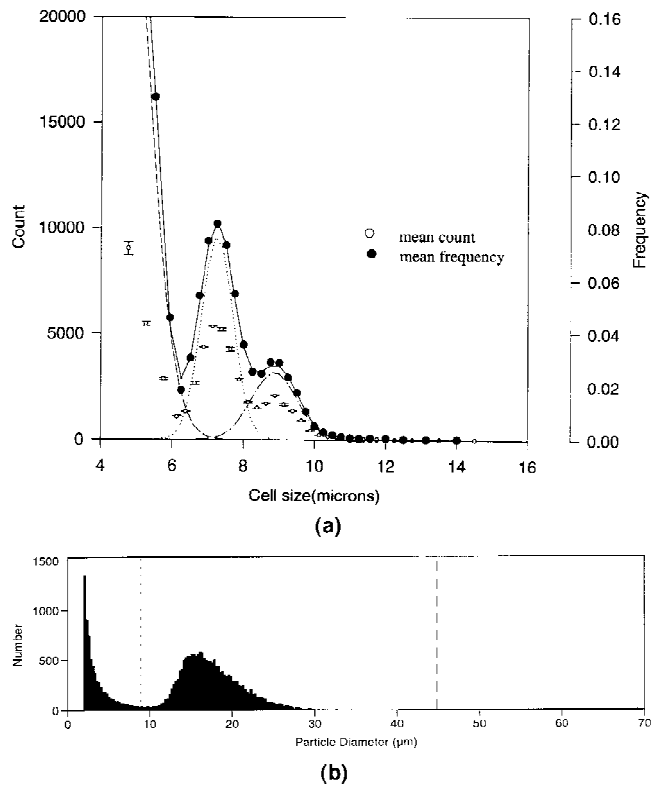


**Figure 3.** Experimental results of cell diameter analysis for human lymphocytes (a) and MCF-7 cells (b). Data for the human lymphocytes are presented as mean cell count ( $\circ$ ) and mean frequency ( $\bullet$ ). Error bars were only included for the mean count data. The various curves represent the fitting of the data to three gaussian-distributed cell populations corresponding, presumably, to red blood cells (peak < 4  $\mu\text{m}$ ), lymphocytes (peak  $\approx 7.2$   $\mu\text{m}$ ), and monocytes (peak  $\approx 9.0$   $\mu\text{m}$ ). (b) Histogram output from the Multisizer software.

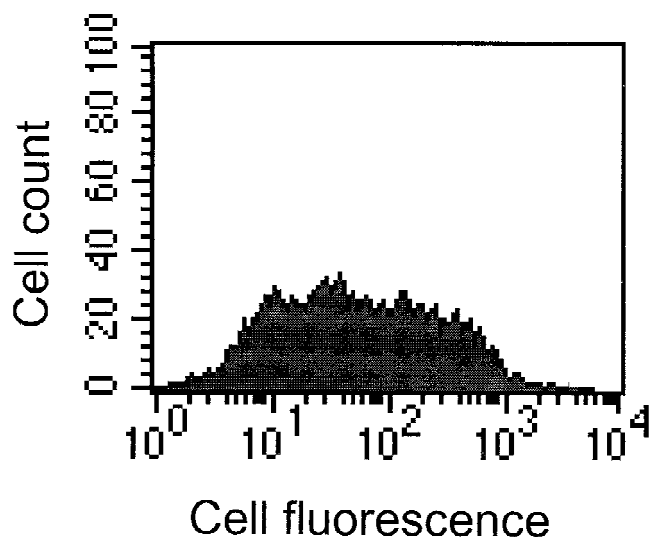
Using a nonlinear root finding technique, three gaussian curves were fit to these data. These curves are indicated by the different dotted lines in Figure 3a. As an internal consistency check, the sum of the three gaussian curves (the solid line) was superimposed on the cell size distribution data, showing a good fit (Fig. 3a). Because we are most interested in the lymphocytes in this analysis, the curve-fitting routine gave a mean diameter of 7.25  $\mu\text{m}$  with a standard deviation of 0.477  $\mu\text{m}$ .

Figure 3b is a representative histogram output using Multisizer AccuComp 1.19 software for the cell diameters of MCF-7 cells. This software automatically calculates a number of statistical measures of the data including mean and standard deviation. A total of seven independent samples, over a range of cell concentrations, were analyzed with the system. No effect of cell concentration was observed and the mean diameter, based on the seven samples, was 17.28  $\mu\text{m}$  with a standard deviation of 3.52  $\mu\text{m}$ . This mean and standard deviation were determined for the data within the dotted, vertical lines indicated in Figure 3b. This range was chosen because the peak at the low end is assumed to be cell debris.

Figure 4 presents a FACS histogram of the MCF-7 cells. Notice the much larger width of positive cell fluorescence peak, when compared with the FACS histograms of the human CD8 lymphocytes. Note, in contrast to the lymphocyte analysis, a single cell line was used, and the background fluorescence of unlabeled cells is not shown.

## MATHEMATICAL MODEL

Because this derivation primarily involves theoretical evaluation of the maximum resolution, with respect to cell sur-



**Figure 4.** Flow-cytometric analysis of MCF-7 cells. The primary antibody used for labeling was a mouse anti-human monoclonal antibody to epithelial membrane antigen (EMA), whereas the secondary antibody was a polyclonal biotin conjugate. Finally, the cells were stained with avidin-FITC label.

face marker density, which can be obtained using colloidal/molecular labels, the actual design and limitations of a practical cell separator will not be discussed.

## Force Balance

The fundamental forces acting on an aqueously suspended, paramagnetically labeled, cell are magnetism, buoyancy, gravity, and drag, designated,  $F_m$ ,  $F_{bou}$ ,  $F_g$ , and  $F_d$ , respectively (Fig. 5). If the Reynolds number is less than 0.1, one can assume that  $F_d$  is represented by the Stokes drag. Mathematically, these forces are defined as follows:

$$F_m = A_c \alpha \beta F_b \quad (1)$$

$$F_{bou} = \frac{(\rho_c - \rho_f) \pi D_c^3 g}{6} \quad (2)$$

$$F_d = 3\pi v_c D_c \eta \quad (3)$$

where  $A_c$  is the surface area of the cell,  $\alpha$  is the number of cell surface markers per membrane surface area,  $\beta$  is the number of antibody magnetic bead complexes bound per marker,  $F_b$  is the magnetic force acting on one antibody magnetic bead complex,  $D_c$  is the diameter of a cell,  $g$  is the acceleration of gravity,  $v_c$  is the velocity of a cell,  $\rho_f$  is the density of the fluid,  $\rho_c$  is the density of a cell, and  $\eta$  is the viscosity of the fluid. Whereas the relationship for  $F_m$  appears relatively straightforward,  $F_b$  is highly nonlinear (except under specialized conditions), and is defined by:

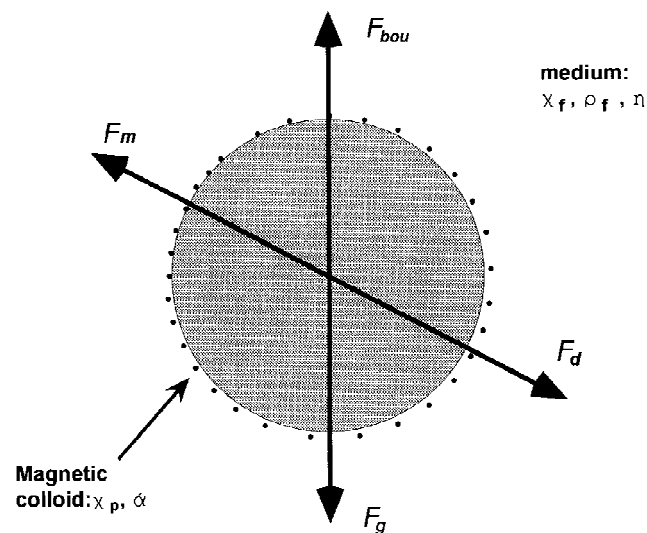


**Figure 5.** Schematic rendering of forces acting on magnetized cells in solution. The fluid is characterized by the magnetic susceptibility,  $\chi_f$ , viscosity,  $\eta$ , and the specific density,  $\rho_f$ . The cell is assumed to be spherical and rigid, and characterized by cell diameter,  $D_c$ . The colloidal magnetic label is uniformly distributed over the cell surface proportional to the surface marker density,  $\alpha$ . The colloid's magnetic susceptibility is  $\chi_p$ . Contribution of magnetic forces acting on magnetic colloid on the cell surface results in the total magnetic force ( $F_m$ ), applied at the center of the cell. Other forces acting on the cell are hydrodynamic drag ( $F_d$ ), gravity, and buoyancy ( $F_{bou}$ ).

$$\mathbf{F}_b = \frac{1}{2\mu_o} \Delta\chi V_b \nabla B^2 \quad (4)$$

where  $\mu_o$  is the magnetic permeability of free space;  $\Delta\chi$  is the difference in magnetic susceptibility between the magnetic bead,  $\chi_b$ , and the surrounding medium,  $\chi_f$  (saline in this case);  $V_b$  is the volume of one magnetic bead, and  $\mathbf{B}$  is the external magnetic field strength (Zborowski, 1997) (note:  $\mathbf{F}_b$  is a vector in the direction of magnetic energy gradient). The magnitude of the vector  $\mathbf{F}_b$  is denoted by  $F_b$  in Eq. (1). The SI unit system is used throughout this study.

### Assumptions

In the derivation that follows, which uses the aforementioned fundamental forces, the following assumptions will be made. First, a direct proportionality exists between the surface marker and the paramagnetic force acting on the label(s); that is,  $\beta$  is a constant. This does not necessarily require a one-to-one correspondence between marker and label; rather, we assume that the magnetic force acting on a labeled marker is the same for any marker on the cell surface. For purposes of this derivation, we will assume that  $\beta = 1$ . Second, there are no flow effects on the magnetically labeled cells, except the drag force, which arises from the magnetically induced velocity. Third, the diffusion coefficient of labeled cells is vanishingly small; that is, there is no thermal or Brownian motion by the cells. Fourth, there are no cell–cell interactions. Fifth, the cell surface marker density,  $\alpha$ , is independent of cell diameter. Sixth, there is no nonspecific binding of antibodies. Finally, there is a constant binding affinity of the antibodies to the surface marker.

### Force Balance

Applying Newton’s second law, and considering for simplicity that the direction of motion is perpendicular to gravity, on obtains the following equation:

$$\mathbf{F}_m + \mathbf{F}_d = m\mathbf{a} \quad (5)$$

where  $m$  is cell mass, and  $a$  is its acceleration. Reddy et al. (1996) demonstrated that, for Dynalbeads, which are several orders of magnitude greater in paramagnetic moment than typical colloidal or molecular labels, that the  $\mathbf{F}_m$  and  $\mathbf{F}_d$  terms are several orders of magnitude greater than the inertial  $m\mathbf{a}$  term. Consequently, it will be assumed that the right-hand side of Eq. (5) can be set equal to zero.

Substituting Eq. (1) and (3) into (5), setting (5) equal to zero, and replacing  $A_c$  by the expression for the surface area of a sphere, and solving for  $v_c$ , one obtains:

$$v_c = \frac{D_c \alpha F_b}{3\eta} \quad (6)$$

Eq. (6) indicates that there are four variables ( $D_c$ ,  $\alpha$ ,  $\eta$ , and  $F_b$ ) that control the velocity of a paramagnetically labeled cell.

### Nondimensionalization of Eq. (6)

One can define the following nondimensional variables:

$$D_c^* = \frac{D_c}{D_{cl}}; v_c^* = \frac{v_c}{v_{cl}}; \mathbf{F}_b^* = \frac{\mathbf{F}_b}{\mathbf{F}_{bl}}; \alpha^* = \frac{\alpha}{\alpha_l}; \sigma^* = \frac{\sigma}{D_{cl}} \quad (7)$$

where  $D_{cl}$  corresponds to approximately one cell diameter ( $1 \times 10^{-5}$  m),  $v_{cl}$  corresponds to a velocity of one cell diameter per second ( $1 \times 10^{-5}$  m/s),  $\mathbf{F}_{bl}$  corresponds to the magnitude of the paramagnetic force acting on one colloidal, paramagnetic bead ( $1.96 \times 10^{-15}$  N), and  $\alpha_l$  corresponds to a typical number of CD8 molecules on a human lymphocyte ( $1 \times 10^5$ ) (Barclay et al., 1993) divided by the surface area on a sphere of diameter  $D_{cl}$  ( $3.18 \times 10^{14}$  marker/m<sup>2</sup>).

Substituting Eq. (7) into Eq. (6), one obtains:

$$v_c^* = \left[ \frac{D_l \alpha_l F_{bl}}{\eta v_l} \right] \frac{D_c^* \alpha^* F_b^*}{3} = \zeta \frac{D_c^* \alpha^* F_b^*}{3} \quad (8)$$

where the nondimensional group,  $\zeta$ , is a ratio of magnetic forces to drag forces.

### Relationship of $v_c^*$ and $\alpha^*$ to Cell Diameter

The key to the type of separation discussed in this article is the exploitation of the velocity difference in cells as a result of differences in the degree to which the cell is labeled, which corresponds to the value of  $\alpha$ , or  $\alpha^*$ . However, as can be observed, the velocity of a cell is directly proportional to the diameter of the cell as well.

Because many characteristics of biological systems exhibit a gaussian, or normal, distribution around a mean value a normal distribution of cell diameters will be assumed (for the purpose of this derivation). When expressed in “standard form,” the following relationship expresses the gaussian distribution around a zero mean (Spiegel, 1996):

$$Y = \frac{1}{\sqrt{2\pi}} e^{-\frac{1}{2}z^2} \quad (9)$$

where  $z$  is defined for this derivation as:

$$z = \frac{(D_c^* - D_{cm}^*)}{\sigma^*} \quad (10)$$

where  $D_{cm}^*$  is the dimensionless, mean cell diameter, and  $\sigma^*$  is the dimensionless standard deviation of cell diameter,  $D_c^*$ , distribution around the mean,  $D_{cm}^*$ . From these two relationships [Eqs. (9) and (10)], one can set a value of  $z$  such that a specific percent of the cell population falls within the cell diameter range ( $D_{cm}^* - z\sigma^*$ ) to ( $D_{cm}^* + z\sigma^*$ ). For example, for a value  $z = 2$ , 95.45% of the given cell population will be included within the cell diameter range of ( $D_{cm}^* - z\sigma^*$ ) to ( $D_{cm}^* + z\sigma^*$ ). [Note: The mean cell diameter must be many times larger than the measure of cell diameter distribution around the mean (i.e., standard deviation) for the gaussian distribution to represent correctly the cell diameter distribu-

tion. If this is not true; then the use of a log-normal distribution is more appropriate.]

Rearranging Eq. (10) and substituting into Eq. (8), and setting  $D_{cm}^* = 1$ , one obtains:

$$\frac{\zeta \alpha^* F_b^*}{3} (1 - z\sigma^*) < v_c^* \leq \frac{\zeta \alpha^* F_b^*}{3} (1 + z\sigma^*) \quad (11)$$

for the range of velocities that a labeled cell can assume for a given value of  $\alpha^*$ , if the cell diameters vary within the range of  $(1 - z\sigma^*) < D_c^* < (1 + z\sigma^*)$ . Note that, if the product  $|z| \cdot \sigma^* \geq 1$ , the cell is stationary in the magnetic field or moves against the magnetic energy gradient. In this analysis, we assume that, for all magnetically labeled cells, the condition  $\Delta\chi > 0$  holds. Consequently, all such cells move in the direction of  $\alpha^*$  of the magnetic energy gradient and, therefore,  $|z| \cdot \sigma < 1$ .

The implications of Eq. (11) are illustrated in Figure 6 as the fraction of cells with a velocity  $v_c^*$  [calculated by integrating over some  $z$  interval, Eq. (9)] versus the cell velocity,  $v_c^*$ , for different values of  $\alpha^* F_b^*$ . As can be observed in Eq. (11), for a specific value of  $\alpha^* F_b^*$ , a range of  $v_c^*$  is possible. In addition, this range of  $v_c^*$  increases as the value of  $\alpha^* F_b^*$  increases.

Because, for a given value of  $\alpha^* F_b^*$ , a range of values of  $v_c^*$  is obtained, using Eq. (11) this range can be determined as a function of  $z$ :

$$\begin{aligned} |\Delta v_c^*| &= \left| \zeta \frac{(1 + z\sigma^*) \alpha^* F_b^*}{3} - \zeta \frac{(1 - z\sigma^*) \alpha^* F_b^*}{3} \right| \\ &= \zeta \frac{\alpha^* F_b^*}{3} 2z\sigma^* \end{aligned} \quad (12)$$

This ‘‘spread’’ of cell velocities, due to the distribution of cell diameters, is analogous to the ‘‘height’’ of a ‘‘theoretical plate’’ discussed elsewhere in distillation, absorption, and chromatography (Foust et al., 1980; King, 1980). Notice that the ‘‘height’’ is proportional to the value of  $\alpha^*$ ,  $F_b^*$ ,

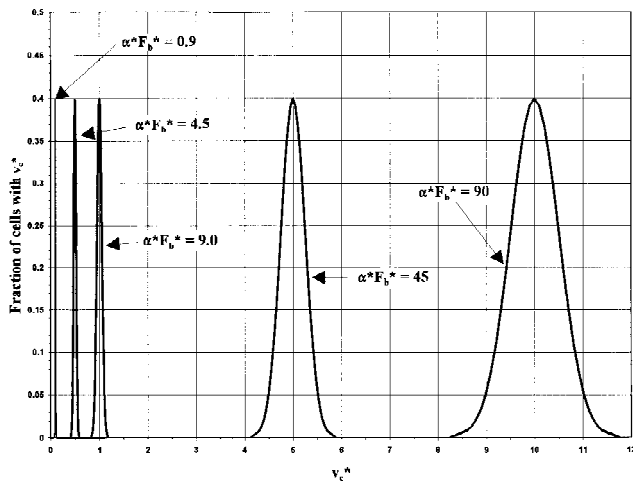


**Figure 6.** Fraction of cells with a velocity  $v_c^*$  versus  $v_c^*$  for a range of values of the product  $\alpha^* F_b^*$ .

$\sigma^*$ , and  $z$ . In this context, the value of  $z$  is a measure of the ‘‘purity’’ of each fraction with respect to the overlap of another  $\alpha^* F_b^*$  distribution.

The same type of analysis can be conducted with respect to  $\alpha^*$ . By rearranging Eq. (8), and replacing  $D_c^*$  with  $(1 \pm z\sigma^*)$ , one obtains:

$$\frac{3v_c^*}{\zeta F_b^* (1 + z\sigma^*)} \leq \alpha^* < \frac{3v_c^*}{\zeta F_b^* (1 - z\sigma^*)}, |z| \cdot \sigma^* < 1 \quad (13)$$

which states that one only predicts a range of values of  $\alpha^*$  on the basis of the measured value of  $v_c^*$ . Again, the range of marker densities predicted for the same cell velocity is due to the distributions of cell diameters,  $D_c^*$ . As with Eq. (12), one can solve for the ‘‘spread’’ of marker concentrations, as a result of the variability of cell diameters, for a given velocity:

$$|\Delta \alpha^*| = \frac{3v_c^*}{F_b^* \zeta} \frac{2z\sigma^*}{1 - z^2 \sigma^{*2}}, |z| \cdot \sigma^* < 1 \quad (14)$$

The second term on the right-hand side can be replaced by  $2z\sigma^*$  for values of  $\sigma$  less than 0.1, because a value of  $\sigma^* = 0.1$  and  $z = 2$  results in only a 4% error and a value of  $\sigma^* < 0.1$  would result in an even smaller error.

## Theoretical Number of Plates

Given the relationships for the ‘‘height’’ of a theoretical plate, represented by  $|\Delta \alpha^*|$  [Eq. (14)], resulting from the degree of uncertainty in the data as a result of the gaussian distribution of cell diameters, it is possible to calculate the number of plates, or in the context of this derivation, the number of individual values of  $\alpha^*$  one can distinguish (with a degree of accuracy determined by  $z$ ) for a particular range of  $v_c^*$ . Two methods will be presented that allow the determination of the number of plates: a graphical approach and an analytical approach.

## Graphical Approach

The graphical approach has some similarities to the graphical approach used in distillation, absorption analysis, and chromatography (Foust et al., 1980; Giddings, 1991). If  $\sigma = 0$  (corresponding to a monodisperse cell suspension), inequalities in Eq. (13) reduce to Eq. (8) (with  $D_{cm}^* = 1$ ) showing a linear relationship between  $\alpha^*$  and  $v_c^*$  going through the origin with a slope of  $3/\zeta F_b^*$ . This is represented by the solid line in Figure 7. For values of  $\sigma^* > 0$  (corresponding to a distribution of cell diameters around certain mean cell diameter), two additional lines can be drawn. One line will have a slope increased by a factor of  $1/(1 - z\sigma^*)$  and the other will have a slope decreased by a factor of  $1/(1 + z\sigma^*)$ , relative to the line with  $\sigma$  equal to zero [Eq. (13); note that  $|z| \cdot \sigma^* < 1$ ]. These lines are called operating lines. Also, as indicated, as  $\sigma^*$  or  $z$  increases, the relative distance of the operating line off the solid line increases.

Once these three lines are drawn, one can find the corresponding value of  $\alpha^*$ , for a given  $v_c^*$ , or coordinates of

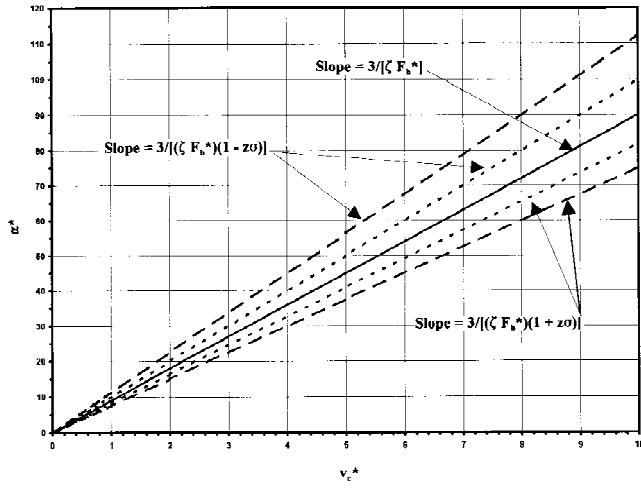


**Figure 7.** Position of operating lines for graphical method for determination of theoretical number of plates.

point A in Figure 8 ( $\alpha_a^*$ ,  $v_{ca}^*$ ), from the solid line. Next, a horizontal line can be drawn through point A. The points of intersection of this horizontal line with the two operating lines correspond to the edges of one “theoretical” plate. Subsequently, a vertical line can be drawn upwards from the highest value of  $v_c^*$  for the particular plate (point C in Fig. 8), until it intersects with the upper operating line. Next, another horizontal line can be drawn until this line intersects with the lower operating line. This corresponds to the next “plate.” This process can be continued in both directions until the limits of the measured values of  $v_c^*$  (lower,  $v_{c0}^*$  and upper,  $v_{cn}^*$ ) are reached.

Several observations regarding this process can be made. First, as can be observed from from Figure 8, the “size” of a “plate” increases with increasing values of  $v_c^*$  and  $\alpha^*$ . Also, the number of “plates” is a function of the value of  $\sigma^*$ . The smaller the value of  $\sigma^*$ , the greater the number of “plates” that can be obtained for a given velocity range. This corresponds to a greater ability to differentiate cells with respect to different values of  $\alpha^*$ .

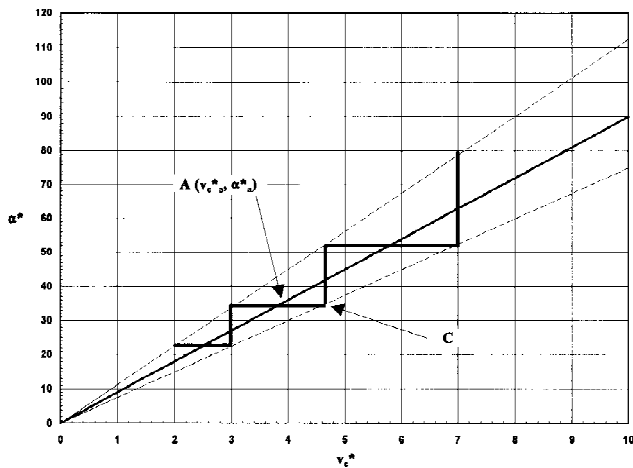


**Figure 8.** Graphical example of theoretical plate calculations.

## Analytical Approach

The theoretical number of plates can also be determined analytically. For a given velocity difference,  $v_{cn}^* - v_{c0}^*$ , if the difference is sufficiently large, one can divide the difference into  $n$  theoretical plates. This is illustrated graphically in Figure 9 (for  $n = 4$ ), and mathematically by:

$$v_4^* - v_0^* = (v_1^* - v_0^*) + (v_2^* - v_1^*) + (v_3^* - v_2^*) + (v_4^* - v_3^*) \quad (15)$$

One can then replace the  $v_n^*$  terms using the following relationships:

$$\begin{aligned} v_{n+1}^* &= \frac{\zeta^* F_b^*}{3} (1 + z\sigma^*) \alpha_n^* \\ &= k_1 \alpha_n^* \cdot v_n^* \\ &= \frac{\zeta^* F_b^*}{3} (1 - z\sigma^*) \alpha_n^* \\ &= k_2 \alpha_n^* \end{aligned} \quad (16)$$

to obtain:

$$k_2(\alpha_4^* - \alpha_0^*) = (k_1 - k_2)\alpha_0^* + (k_1 - k_2)\alpha_1^* + (k_1 - k_2)\alpha_2^* + (k_1 - k_2)\alpha_3^* \quad (17)$$

Making the substitution:

$$\begin{aligned} (k_1 - k_2) &= \left[ \frac{\zeta^* F_b^*}{3} (1 + z\sigma^*) - \frac{\zeta^* F_b^*}{3} (1 - z\sigma^*) \right] \\ &= \frac{\zeta^* F_b^*}{3} 2z\sigma^* \\ &= C \end{aligned} \quad (18)$$

into Eq. (17) one obtains:

$$k_2(\alpha_4^* - \alpha_0^*) = C\alpha_0^* + C\alpha_1^* + C\alpha_2^* + C\alpha_3^* \quad (19)$$

Next,  $\alpha_1^*$  can be replaced by the following function of  $\alpha_0$ :

$$\alpha_1^* = \frac{v_1^*}{k_2} = \frac{k_1}{k_2} \alpha_0^* = K\alpha_0^* \quad (20)$$

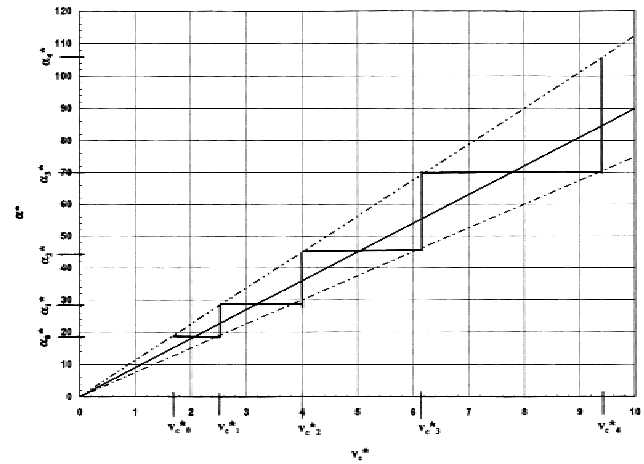


**Figure 9.** Position for four plates used in the derivation of analytical solution to the theoretical number of plates. In this example,  $z = 2$ ,  $\sigma = 0.05$ , and  $\zeta = 1$ .

where  $K = k_1/k_2$ . Eq. (20) can be generalized to:

$$\alpha_m^* = K^m \alpha_0^* \quad (21)$$

Substituting Eq. (21) into Eq. (19) one obtains:

$$k_2(\alpha_4^* - \alpha_0^*) = C\alpha_0^* + CK\alpha_0^* + CK^2\alpha_0^* + CK^3\alpha_0^* \quad (22)$$

Rearranging, Eq. (22) becomes:

$$\frac{k_2}{C\alpha_0^*} (\alpha_4^* - \alpha_0^*) = [1 + K + K^2 + K^3] \quad (23)$$

Given the geometric series:

$$b + br + br^2 + br^3 + \dots + br^{n-1} = \frac{b(1-r^n)}{1-r} \quad (24)$$

one can replace the right-hand side of Eq. (23) with Eq. (24) to obtain:

$$\frac{k_2}{C\alpha_0^*} (\alpha_4^* - \alpha_0^*) = \frac{1-K^4}{1-K} \quad (25)$$

Generalizing, and solving for the “ $n$ ” plate, one obtains:

$$n = \frac{\ln \left[ 1 - (\alpha_n^* - \alpha_0^*)(1-K) \frac{k_2}{C\alpha_0^*} \right]}{\ln K} \quad (26)$$

Substituting back the definitions of  $K$ ,  $k_2$ , and  $C$ , and simplifying, one obtains:

$$n = \frac{\ln \left[ \frac{\alpha_n^*}{\alpha_0^*} \right]}{\ln \left[ \frac{1+z\sigma^*}{1-z\sigma^*} \right]} = \frac{\ln \left[ \frac{v_n^*}{v_0^*} \right]}{\ln \left[ \frac{1+z\sigma^*}{1-z\sigma^*} \right]}; \quad |z\sigma^*| < 1 \quad (27)$$

Eq. (27) indicates that the number of theoretical plates is a function of only the ratio of  $\alpha_n^*/\alpha_0^*$  or  $v_n^*/v_0^*$  and the values of  $z$  and  $\sigma^*$ , such that the condition  $|z\sigma^*| < 1$  is true.

Figure 10 is a plot of Eq. (27) for the number of theoretical plates,  $n$ , as a function of the ratio  $\alpha_n^*/\alpha_0^*$  for different values of the product,  $z\sigma^*$ .

## DISCUSSION

The preceding analysis provides a theoretical limit for the number of fractions into which an immunomagnetically labeled cell suspension can be divided. An interesting observation of Eq. (27) is the lack of a magnetic force term, which implies that the number of plates is independent of magnetic force applied to separate the cells. This is in contrast to relationships that define the number of theoretical plates needed in chromatography or electrophoresis. For both these types of separation, Giddings (1991) commented on how the theoretical number of plates is proportional to the ratios of two energies: “ $-\Delta\mu^{ext}$ , the energy which cre-

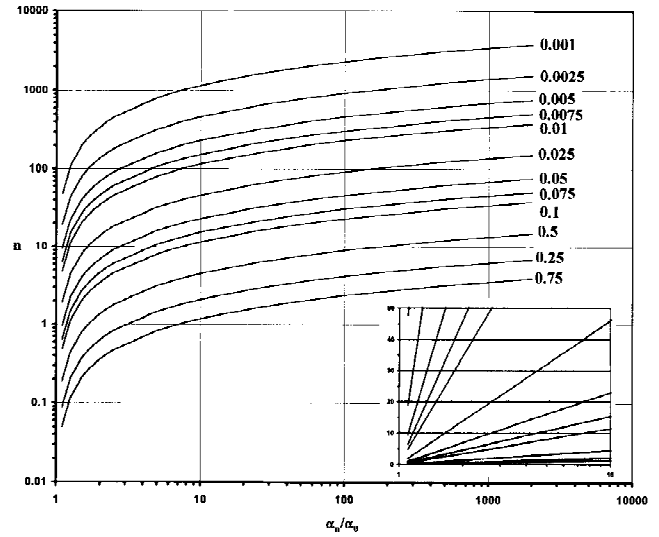


Figure 10. Plot of Eq. (27) for the number of theoretical plates,  $n$ , as a function of the ratio  $\alpha_n^*/\alpha_0^*$  for different values of the product,  $z\sigma^*$ .

ates and structures the separation, and thermal energy,  $RT$  (times  $2\theta$ ), which drives the diffusion that dissipates the separation.” Mathematically, the number of theoretical plates,  $N$ , is represented by:

$$N = \frac{-\Delta\mu^{ext}}{2\theta RT} \quad (28)$$

This observation, namely the lack of dependence of the theoretical number of plates on the driving force of the magnetic separation, can best be described by understanding that: (1) the “randomizing energy” is based on cell size distribution, not thermal energy; and (2) as Eq. (6) indicates, the magnetic force acting on the cell,  $F_m$ , is directly proportional to both the “randomizing” term,  $D_c$ , and the cellular separation term,  $\alpha$ . Consequently, as  $F_b$  increases, the velocity “spread” due to the “randomizing” effect of the distribution of cell diameters also increases (see Fig. 6).

The results in Figures 1 and 4 indicate that a large range of marker densities exists, if one makes the assumption that a proportionality exists between fluorescence antibody tag and cell surface marker. Making the assumptions that: (i) a  $10^2$  range in marker density exists in the CD8 lymphocytes, which is equivalent to mathematically stating the ratio  $\alpha_n^*/\alpha_0^* = 10^2$  (or a ratio in maximum and minimum velocity,  $v_n^*/v_0^* = 10^2$ ); (ii) the nondimensionalized standard deviation,  $\sigma^*$ , of the cell diameter is 0.051; and (iii) choosing a value of  $z = 2$ , then Eq. 27 or Figure 10 indicates that 22.5 “theoretical plates” are possible. In other words, for a 95.5% confidence that a given “plate” contains cells with a marker density of a given value, 22.5 fractions of CD8 lymphocytes differing in marker densities can be theoretically obtained.

Visual inspection of Figure 4 indicates that, for the MCF-7 cells, a  $10^3$  range in marker density exists, which is equivalent to stating mathematically the ratio  $\alpha_n^*/\alpha_0^* = 10^3$ . However, because the nondimensionalized standard deviation,  $\sigma^*$ , of the cell diameter is 0.352, for a value of  $z = 2$ , Eq. (27) or Figure 10 indicate that only 4.0 theoretical plates can be obtained. This large reduction in the number of theoretical plates, despite the factor of ten increase in range of marker density, indicates the importance of the distribution of cell diameters in this analysis (standard deviation of the MCF-7 cells is 6.4 times greater than lymphocytes). It should be noted that visual, microscopic observations of these cells confirm the Coulter Counter data that there is, in fact, a large range in cell diameters. Moreover, visual microscopic observation of cell motion in the magnetic field (unpublished) shows significant differences between velocities of cells of the same size thus qualitatively verifying the assumption that cell surface marker density is independent of cell surface area.

In our current analysis, a normal distribution was used to describe distributions of diameters of human lymphocytes (Fig. 3). However, a log-normal distribution for highly dispersed cells size might be more appropriate (such as the MCF-7 cell line). Future work will consider both types of distribution.

Several significant assumptions were made in this derivation. A major assumption, which comprises several of the assumptions stated previously, relates to the concept of a direct proportionality between marker density and the degree to which a cell is paramagnetically labeled. This situation is not unique. As discussed in the Introduction, quantitation of fluorescence with respect to surface marker density in FACS analysis has been and is continuing to be conducted (Bikoue et al., 1996). We are developing a “next generation” analysis device, based on the initial device developed by Reddy et al. (1996) in which individual, magnetically labeled cells are microscopically recorded, as they move through a known magnetic field. These recorded images are then analyzed by computer and quantified, in a statistically meaningful way, to determine both the mean and distribution of paramagnetic labels on cells. This device will allow optimization studies to be conducted on the labeling protocols as well as a variety of other tests and controls.

A second assumption is the lack of flow effects except for drag. Ongoing research in our laboratories (Zborowski et al., 1997a, 1997b) is developing devices that can “fractionate” immunomagnetically labeled cells, with respect to a particular cell surface marker. With these devices, various flow effects on the ability to achieve the theoretical number of plates, are being investigated.

The final significant assumption is that marker density is independent of cell diameter (cell surface area). This assumption has been well documented by Shapiro (1995) for selected cell types. Using the modified technique of Reddy et al. (1996), discussed earlier, and cell size analysis by Coulter Counter, this assumption will be tested extensively.

## NOMENCLATURE

$A_c$	surface area of a cell ( $m^2$ )
$a$	acceleration ( $m/s^2$ )
$B$	magnetic flux density (Tesla)
$C$	$k_1 - k_2$
$D_c$	cell diameter (m)
$D_{cm}$	mean cell diameter (m)
$D_{cl}$	characteristic length ( $1 \times 10^{-5}$ m)
$F_m$	magnetic force vector
$F_m$	magnitude of magnetic force
$F_b$	magnitude of magnetic force per antibody microbead complex
$F_{bt}$	magnitude of characteristic magnetic force per antibody-bead complex ( $1.96 \times 10^{-15}$ N)
$F_{bou}$	magnitude of the force of buoyancy (N)
$F_d$	magnitude of the force of drag (N)
$g$	force of gravity ( $m/s^2$ )
$k_1$	$\zeta F_b^*/3 (1 + z\sigma)$
$k_2$	$\zeta F_b^*/3 (1 - z\sigma)$
$K$	$k_1/k_2$
$m$	cell mass (kg)
$n$	number of theoretical plates
$R$	gas constant
$V_b$	volume of paramagnetic bead ( $m^3$ )
$v_c$	velocity of a cell (m/s)
$v_l$	characteristic velocity ( $1 \times 10^{-5}$ m/s)

### Greek letters

$\alpha$	number of specific markers/unit surface area of cell ( $3.18 \times 10^{14}/m^2$ )
$\beta$	number of antibody magnetic bead complexes bound per marker
$\zeta$	ratio of magnetic forces to drag forces
$\pi$	pi
$\rho_f$	density of fluid
$\chi_b$	magnetic susceptibility of a magnetic bead
$\chi_f$	magnetic susceptibility of the surrounding medium
$\Delta\chi$	$(\chi_b - \chi_f)$
$\mu_o$	magnetic permeability of free space ( $4\pi \times 10^{-7}$ Tm/A)
$\eta$	viscosity of water ( $1 \times 10^{-3}$ kg/m · s)
$\sigma$	standard deviation of cell diameters (m)

### Superscripts

*	nondimensional form
---	---------------------

### Subscripts

$l$	characteristic values
$o$	lowest value of variable
$n$	highest value of variable

## References

- Barclay, A. N., Birkeland, M. L., Brown, M. H., Beyers, A. D., Davis, S. J., Somoza, C., Williams, A. F. 1993. The leukocyte antigen facts book. Academic Press, San Diego, CA.
- Bazylinski, D. A., Frankel, R. B., Jannasch, H. W. 1988. Aerobic magnetite production by a marine, magnetotactic bacterium. *Nature* **334**: 518–519.
- Bikoue, A., George, F., Poncelet, P., Mutin, M., Janossy, G., Sampol, J. 1996. Quantitative analysis of leukocyte membrane antigen expression: normal adult values. *Cytometry* **26**: 137–147.
- Bohmer, R., Papaioannou, J., Ashcroft, R. 1985. Flow cytometric determination of fluorescence ratios between differently stained parameters is dependent on excitation intensity. *J. Histochem. Cytochem.* **33**: 974–976.

- Busch, J., Huber, P., Pflüger, E., Miltenyi, S., Holtz, J., Radbruch, A. 1994. Enrichment of fetal cells from maternal blood by high gradient magnetic cell sorting (double MACS) for PCR-based genetic analysis. *Prenatal Diagn.* **14**: 1129–1140.
- Chatelier, R., Ashcroft, R. 1987. Calibration of flow cytometric fluorescence standards using the isoparametric analysis of ligand binding. *Cytometry* **8**: 632–636.
- Foust, A. S., Wenzel, L. A., Clump, C. W., Maus, L., Andersen, L. B. 1980. Principles of unit operations. 2nd edition. John Wiley & Sons, New York.
- Giddings, J. C. 1991. Unified separation science. John Wiley & Sons, New York.
- King, C. J. 1980. Separation processes. McGraw-Hill, New York.
- Klaus, G. G. B. 1987. Lymphocytes: a practical approach. IRL Press, Oxford.
- Mansour, V., Weiler, M., Gee, A. P. 1992. Factors limiting the efficiency of immunomagnetic cell separation, pp. 169–179. In: S. Gross, A. P. Gee, and D. A. Worthington-White (eds.), *Advances in bone marrow purging and processing*. Wiley-Liss, New York.
- Manyonda, I. T., Soltys, A. J., Hay, F. C. 1992. A critical evaluation of the magnetic cell sorter and its use in the positive and negative selection of CD45RO+ cells. *J. Immunol. Meth.* **149**: 1–10.
- Meldrum, F. C., Mann, S., Heywood, B. R., Frankel, R., Bazylinski, D. 1993. Electron microscopy study of magnetosomes in a cultured magnetotactic bacteria. *Proc. Royal Soc. London Series B* **251**: 231–236.
- Miltenyi, S., Müller, W., Weichel, W., Radbruch, A. 1990. High gradient magnetic cell separation. *Cytometry* **11**: 231–238.
- Okazaki, M., Maeda, N., Shiga, T. 1986. Drift of an erythrocyte flow line due to the magnetic field. *Experientia* **42**: 842–845.
- Parks, D., Bigo, M., Moore, W. 1988. Logarithmic amplifier transfer function evaluation and procedures for logamp optimization and autocorrection. *Cytometry* **155**: 27.
- Pauling, L., Coryell, C. D. 1936. The magnetic properties and structure of hemoglobin, oxyhemoglobin and carbonmonoxyhemoglobin. *Proc. Natl. Acad. Sci.* **22**: 210–216.
- Poncelet, P., Bikque, A., Lavabre, T., Poinès, G., Parant, M., Duperray, O., Sampol, J. 1991a. Quantitative expression of human lymphocytes membrane antigens: definition of normal densities measured in immunocytometry with the QIFI assay. *Cytometry* **5**(suppl.): 82–83.
- Poncelet, P., Carayon, P. 1985. Cytofluorometric quantification of cell-surface antigens by indirect immunofluorescence using monoclonal antibodies. *J. Immunol. Meth.* **85**: 65–74.
- Poncelet, P., Mutin, M., Burnet, O., George, F., Ambrosi, P., Sampol, J. 1991b. Quantification of cell membrane antigenic sites in immunocytometry with indirect IF: the QIFI assay. *Cytometry* **5**(suppl.): 82.
- Radbruch, A., Mechtold, B., Thiel, A., Miltenyi, S., Pflüger, E. 1994. High-gradient magnetic sorting. *Meth. Cell Biol.* **42**: 387–403.
- Reddy, S., Moore, L., Zborowski, M., Chalmers, J. J. 1996. Determination of the magnetic susceptibility of labeled particles by video imaging. *Chem. Eng. Sci.* **51**: 947–956.
- Rubbi, C. P., Patel, D., Rickwood, D. 1993. Evidence of surface antigen detachment during incubation of cells with immunomagnetic beads. *J. Immunol. Meth.* **166**: 233–241.
- Schmitz, B., Radbruch, A., Kümmel, T., Wickenhauser, C., Korb, H., Hansmann, M. L., Thiele, J., Fischer, R. 1994. Magnetic activated cell sorting (MACS)—a new immunomagnetic method for megakaryocytic cell isolation: comparison of different separation techniques. *Eur. J. Haematol.* **52**: 267–275.
- Shapiro, H. M. 1995. Practical flow cytometry. 3rd edition. Wiley-Liss, New York.
- Spiegel, M. R. 1996. Schaum's outline of theory and problems of statistics. 2nd edition. McGraw-Hill, New York.
- Thomas, T. E., Abraham, S. J. R., Otter, A. J., Blackmore, E. W., Lansdorp, P. M. 1992. High gradient magnetic separation of cells on the basis of expression levels of cell surface antigens. *J. Immunol. Meth.* **154**: 245–252.
- Vogt, R. F., Cross, G. D., Henderson, L. O., Phillips, D. L. 1989. Model systems evaluating fluorescein-labeled microbeads as internal standards to calibrate fluorescence intensity on flow cytometers. *Cytometry* **10**: 294–302.
- Vogt, R. F., Cross, G. D., Phillips, D. L., Henderson, L. O., Hannon, W. H. 1991. Interlaboratory study of cellular fluorescence intensity measurements with fluorescein-labeled microbead standards. *Cytometry* **12**: 525–536.
- Zborowski, M. 1997. Physics of the magnetic cell sorting, pp. 205–231. In: U. Hafeli, W. Schutt, J. Teller, and M. Zborowski (eds.), *Scientific and clinical applications of magnetic microcarriers: an overview*. Plenum Press, New York.
- Zborowski, M., Fuh, C. B., Green, R., Baldwin, N. J., Reddy, S., Douglas, T., Mann, S., Chalmers, J. J. 1996. Immunomagnetic isolation of magnetoferritin-labeled cells in a modified ferrograph. *Cytometry* **24**: 251–259.
- Zborowski, M., Moore, L. R., Liping, S., Chalmers, J. J. 1997a. Continuous-flow magnetic cell sorting using soluble immunomagnetic label, pp. 247–260. In: U. Hafeli, W. Schutt, J. Teller, and M. Zborowski (eds.), *Scientific and clinical applications of magnetic microcarriers: an overview*. Plenum Press, New York.
- Zborowski, M., Williams, P. S., Sun, L., Moore, L. R., Chalmers, J. J., 1997b. Cylindrical split and quadrupole magnetic field in applications to continuous-flow magnetic cell sorting. *J. Liquid Chromatogr. Rel. Techn.* **20**: 2887–2905.